WELDING RESEARCH

SUPPLEMENT TO THE *WELDING JOURNAL*, NOVEMBER 2015
Sponsored by the American Welding Society and the Welding Research Council

Disaggregated Metal and Carbide Catchment Efficiencies in Laser Cladding of Nickel-Tungsten Carbide

Using a CO_2 laser, the effects of power, powder feed rate, and travel speed were studied to determine their influence on the efficiency of depositing a nickel tungsten carbide clad coating

BY G. WOOD AND P. F. MENDEZ

ABSTRACT

Composite coatings made of nickel matrix reinforced with tungsten carbide particles are one of the dominant wear-protection systems in mining, oil, and gas applications. In these applications, the balance of powders forming the final coatings is crucial to the final product. This paper presents for the first time an analysis of powder utilization efficiency ("catchment efficiency") where the metallic powders (mostly nickel) and tungsten carbide are discriminated. Experiments were performed using a CO_2 laser system with coaxial powder deposition, and the effects of power, powder feed rate, and travel speed were tested. The metal efficiency was higher than the carbide in all tests. Increasing laser power resulted in increased efficiency for both metal and carbide. Increasing powder feed rate decreased nickel efficiency and increased carbide efficiency, with the overall powder efficiency being approximately constant. Increasing travel speed resulted in strong reduction of efficiency for both carbide and nickel.

KEYWORDS

• Cladding • Hardfacing • Composite Coatings • Metal Matrix Composites

Introduction

Powder-based welding processes such as laser cladding or plasma arc welding (PAW), also referred to as plasma transferred arc welding (PTAW), are the industry standard for depositing tungsten carbide-based wear-resistant coatings (Ref. 1). The dimensions, performance, and cost of the final coating or cladding are directly dependent on the amount of free-flight powder that adheres to the molten surface of the cladding pool contributing to the cladding buildup (Refs. 1–3). Not all of the powders that exit the head end up as part of the cladding bead; the fraction of powders that do is termed the "catchment efficiency" by practitioners.

The focus of this analysis is the efficiency in laser deposition of nickel tungsten carbide (Ni-WC) cladding. The Ni-WC powder blend contains a primary Ni powder (referred to hereafter as metal powder), which solidifies to create the matrix, and ceramic tungsten carbide particles, which in turn serve as the wear-resistant phase in the cladding. The carbide must remain unmelted during the cladding process, contrary to most other wear protection alloys, such as chromium carbide where the reinforcing phase forms in-situ during solidification. Although the microstructural aspects of the Ni-WC are not a focus of this analysis, it is important to note the WC symbol in Ni-WC does not directly refer to the stoichiometric 1:1 form of the carbide only and is used interchangeably with WC, W_2C, and the nonstoichiometric WC_{1-x}.

There have been various contributions to the understanding of catchment efficiency in literature, which can be grouped into two categories: models of catchment efficiency, and experimental exploration of laser parameters to optimize efficiency.

Among models of efficiency, Picasso et al. developed a numerical algorithm to compute powder efficiency, accounting for the angular dependence of laser power absorption and the melt pool shape based on a Gaussian heat distribution (Ref. 4). Lin and Steen presented a model of efficiency based on the geometry of the powder stream at the nozzle focus point, molten pool, and the degree of overlap between the powder stream and molten pool (Ref. 5). Frenk et al. proposed a model of efficiency for off-axis laser cladding with a theoretical maximum mass efficiency of 69%, which was experimentally

G. WOOD (gentry@ualberta.ca) *and P. F. MENDEZ are with Canadian Centre for Welding and Joining, Chemical and Materials Engineering, University of Alberta, Edmonton, AB.*

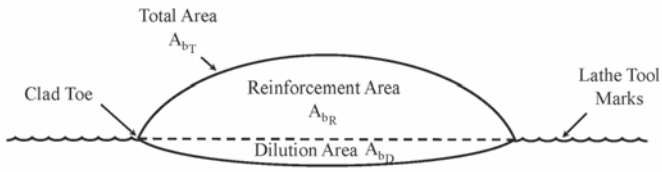

Fig. 1 — Schematic of a cross section of a deposited cladding bead from the experiments.

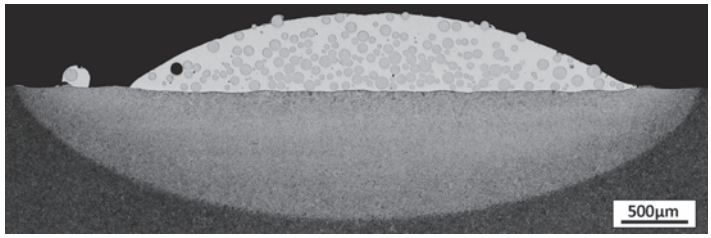

Fig. 3 — Cross section of Bead 3 etched with 3% Nital for 5 s.

Fig. 2 — Laser cladding during the Bead 3 run.

Fig. 4 — Python script output showing carbide area for Bead 3.

validated (Ref. 6). Partes studied the effects of melt pool geometry and nozzle alignment on catchment efficiency taking into account particle time of flight and surface melting under the beam (Ref. 7).

Researchers that have studied parameter optimization for laser cladding of homogeneous alloys include Olivera et al. who analyzed the effect of laser power, powder feed rate, and substrate travel speed on powder efficiency and proposed experimentally determined correlations to fit 316L stainless steel cladding trials (Ref. 8). Gremaud et al. determined the optimal efficiency for thin-walled structures made of single-stacked laser cladding beads. This work explored the effect of travel speed and powder feed rate on the efficiency for a variety of alloys (Ref. 9). A select few researchers have also studied the efficiency of laser cladding of Ni-WC.

Powder efficiency in Ni-WC laser cladding is relatively unexplored. Zhou et al. studied the effect of laser spot dimensions with laser induction hybrid cladding on the efficiency of Ni-WC coatings, but did not directly report values for efficiency. Increases in bead width and height were qualitatively correlated to increased capture efficiency (Ref. 10). Angelastro et al. optimized the process parameters of power, powder feed rate, and travel speed for a multilayer clad of Ni-WC with Co and Cr additions reporting only an overall value for deposition efficiency (Ref. 11). Of the researchers who have measured and modelled efficiency, most have used homogeneous single-component powder feeds, and for those who have directly worked with Ni-WC, none have discriminated between components. This work presents for the first time a detailed analysis of individual component efficiencies for a mixed powder feed, linking the mass capture of two types of immiscible powders to measurable quantities of the process and the cross section of the deposited clad. In this work, laser power, powder feed rate, and travel speed are varied to study the effects on carbide and metal powder catchment efficiency independently.

Experimental Setup

Laser Cladding Equipment

For the experimental trials performed here, the power source was a 6-kW CO_2 laser assembly with water-cooled copper-mirror optics. The focal distance of the final beam-focusing mirror was 345 mm (13.959 in.), and cladding was performed 19 mm (0.75 in.) out of focus beyond the focal point, conforming to typical industrial practices. The laser spot diameter at this working distance was 6.13 mm. A disk powder feeder was used to meter powder to the cladding nozzle with a set Ar carrier gas flow rate of 6.5 L/min. The cladding nozzle was a coaxial production nozzle capable of feed rates up to 150 g/min through a series of 50 equally spaced ports between two concentric conical guides. Argon shield gas flow rate was 1.27 m^3/h. The substrate positioning system is a CNC-controlled x-y lathe bed with a mounted four jaw check headstock and tailstock spindle support. Surface rotation speeds were programmed into the CNC system for a given diameter substrate. For the precision equipment used, it was considered that the actual rotation speed matched its set point.

Powder Feed

The powder feed used in this analysis was a mixture of cast spherical-fused tungsten carbide and a Ni-Cr-B-S blend of metal, which comprise the metal matrix in the deposited cladding. The carbide chemistry reported by the powder supplier was 3.8 wt-% C and the balance W, which corresponds to a stoichiometry of $WC_{0.6}$. The two component powders were mixed together in 60–40% weight fractions of carbide to metal powder, respectively. Size range, reported manufacturer hardness range, weight fractions, and densities are listed in Table 1. The density of the WC_{1-x} carbides is analyzed in Appendix A.

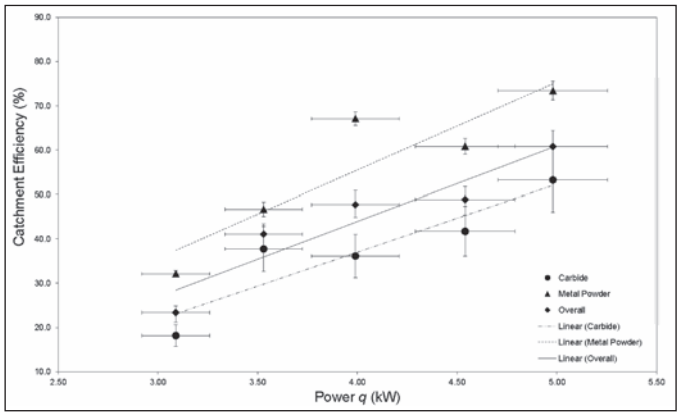

Fig. 5 — Effect of power on catchment efficiency.

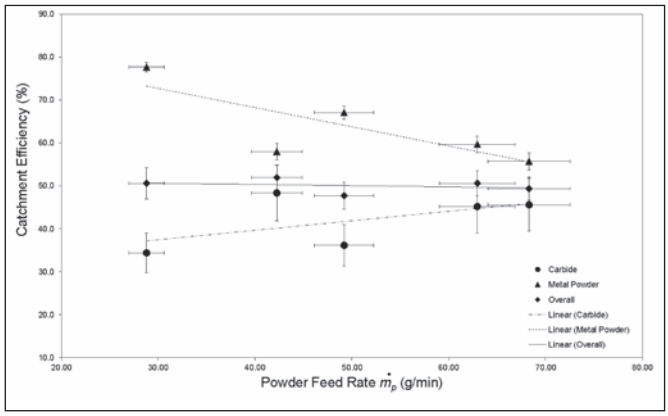

Fig. 6 — Effect of powder feed rate on catchment efficiency.

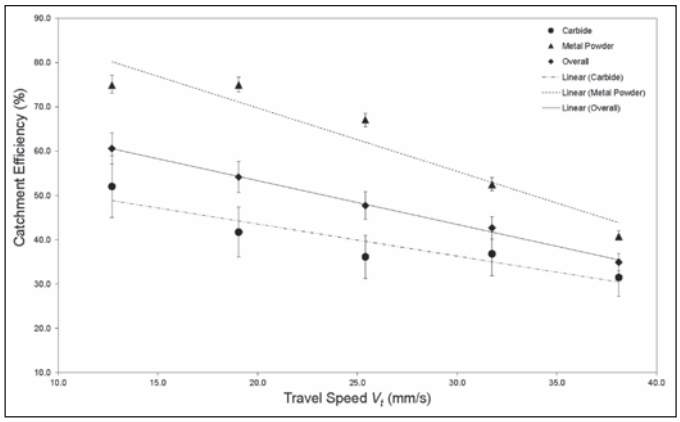

Fig. 7 — Effect of travel speed on catchment efficiency.

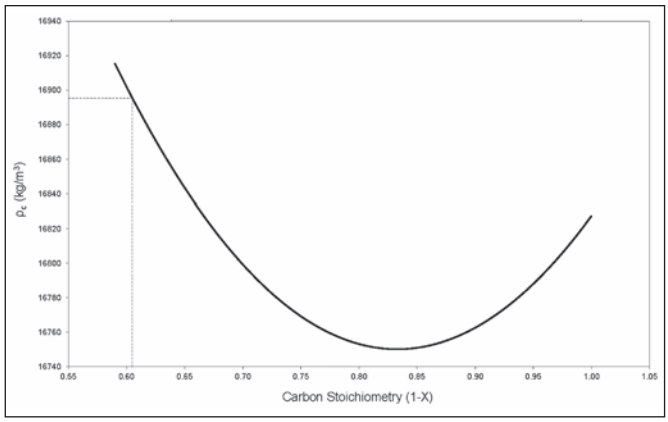

Fig. 8 — Density of WC_{1-Z} as a function of C stoichiometry.

Table 1 — Properties of Powders Used in the Experiments

Component	Size Range (μm)	Expected Hardness Range After Deposition (HV)	Weight Fraction W_f (%)	Density ρ (kg/m^3)
Carbide Powder	45–106	2700–3500	62.60	16,896
Metal Powder	53–150	425	37.40	8100

Sample Preparation

Individual beads were sectioned using a wet saw, mounted, polished to a 0.04-mm finish, and etched for 5 s with 3% Nital to reveal the HAZ. Photomicrographs of the sample cross sections were stitched together to create panoramas of the total bead area and HAZ using Adobe Photoshop™. The reinforcement area A_{bR}, dilution area A_{bD}, and total area A_{bT} were measured by analyzing pixels of the selected region and converting pixel measurements to an actual area using the image scale bar calibrated to a known length. Due to the presence of machining marks on the sample surface, a straight line drawn between the clad toes was used to divide above and below surface levels. These areas and features are shown in Fig. 1.

The area fraction of the carbide was measured using an internally developed Python™ script that identified the carbide based on color contrast with the matrix. The clad area was isolated from the picture and the contrast was adjusted using Photoshop to improve the distinction between the two phases.

Cladding Procedure

The test claddings were performed on a 254-mm-long, 20.3-mm-thick, 165-mm outer diameter 4145 MOD cylindrical bearing substrate. The loaded sample was rotationally centered to within 25 mm (0.001 in.) using an alignment dial indicator. The surface of the bearing was prepared with an initial acetone wash to remove any oil or grease, followed by manual grinding between passes to remove any remaining debris. Conforming to the existing direct carbide application procedures, a 533 K preheat was applied to the rotating substrate using a propane torch. The temperature was checked before each pass using a touch thermocouple at the 0-, 90-, 180-, and 270-deg positions on the cylinder along the rotation direction. These temperature measurements were performed along the centerline of the upcoming bead. Some variation in preheat temperatures was observed across the four measured points, but values within 25 K of each other and the target preheat temperature were taken as acceptable.

The laser power, powder feed, and substrate rotation were programmed to begin simultaneously with the shut-

ter closed to momentarily delay the start of cladding and allow the parameters time to ramp up to test levels. After a five-second waiting period, the shutter was opened and the cladding begun. A 360-deg bead was deposited with no pitch followed immediately by a 2-mm pitch and 180-deg overlapping bead without interruption. The overlapping beads were included to provide bead-on-bead samples for future analysis and are not included as part of this study. Beads were placed 51 mm (2 in.) away from the edges of the coupon to prevent heat accumulation effects. A 12.7-mm (0.5-in.) gap between bead centers was left to allow adequate room for sectioning. Once the half circumference overlapping bead was finished, the shutter was closed, effectively stopping the clad process while the laser power and powder feed rate ramped down. The travel speed was set to shift rapidly to its maximum (25 deg/s) to complete the second full rotation and place the starting point directly beneath the nozzle. Figure 2 shows an example of the in-process Ni-WC clad deposit.

The laser power and powder feed rates were calibrated at the beginning of the experiment and before trials with a parameter change to confirm levels at the substrate. Laser power was measured using a 10-kW Comet 10K-HD power probe, which acts as a copper calorimeter for one second laser exposures. Feed rate was measured by manually capturing the powder flow rate for t_p = 2 min, measuring the accumulated mass, and reporting a per-minute average rate. This calibration is necessary to link the rotation speed of the disk feeder to the actual mass flow rate.

Experimental Matrix

The parameters tested were laser power, power feed rate, and travel speed. These parameters were chosen because there is direct control over them, and they are known to have a large influence on the laser cladding operation.

The matrix has a center point (Bead 3) and two higher and two lower points for each parameter, totalling 13 experiments. Corners were omitted to reduce the number of experiments that would otherwise grow exponentially. Interaction effects between parameters cannot be assessed with the experimental matrix used, but these interactions do not affect the conclusion obtained. The experimental design test run order was randomized to eliminate procedural bias. This was done by assigning each trial a randomly generated number and arbitrarily sorting low to high. Recorded test measurements of each parameter are shown in Table 2.

Table 2 — Experimental Matrix for Cladding of Ni-WC onto a 4145 MOD Substrate for All Beads

Bead Number	Laser Power q (kW)		Powder Feed Rate $\dot{m}_p$ (g/min)		Target Travel Speed V_t		Average Preheat (°C)
	Target	Measured	Target	Measured	(in./min)	(mm/s)	Measured
Bead 1[a,b]	5.0	4.98	50	49.20	60	25.40	257
Bead 2[a]	3.0	3.09	50	49.20	60	25.40	257
Bead 3[a]	4.0	3.99	50	49.20	60	25.40	261
Bead 4	4.0	3.99	50	49.20	45	19.05	258
Bead 5[b]	4.0	3.99	30	28.80	60	25.40	268
Bead 6[b]	4.0	3.99	50	49.20	75	31.75	264
Bead 7[a]	4.5	4.54	50	49.20	60	25.40	263
Bead 8[a]	3.5	3.53	50	49.20	60	25.40	264
Bead 9[a]	4.0	3.98	50	49.20	30	12.70	263
Bead 10[b]	4.0	3.98	60	62.95	60	25.40	264
Bead 11[b]	4.0	3.98	40	42.25	60	25.40	264
Bead 12	4.0	3.98	50	49.20	90	38.10	267
Bead 13[b]	4.0	3.98	70	68.30	60	25.40	263

(a) Laser power measurement performed immediately before test.
(b) Powder feed rate measurement performed immediately before test.
Target preheat was 260°C (500°F).

Table 3 — Bead Area and Carbide Volume Fraction Measurements for Experimental Test Beads

Bead Number	Total Area A_{bT} (mm²)	Reinforcement Area A_{bR} (mm²)	Carbide Volume Fraction fv_{cb} (%)
Bead 1	1.89	1.65	33.64
Bead 2	0.72	0.68	30.05
Bead 3	1.52	1.40	28.48
Bead 4	2.27	2.11	29.30
Bead 5	1.19	0.85	20.27
Bead 6	1.02	0.95	34.42
Bead 7	1.46	1.38	34.29
Bead 8	1.19	1.12	38.04
Bead 9	3.59	3.42	34.71
Bead 10	1.90	1.79	36.39
Bead 11	1.37	1.16	36.26
Bead 12	0.67	0.65	37.48
Bead 13	1.96	1.88	38.56

Determination of Catchment Efficiency

The derivations for carbide, metal powder, and total catchment efficiency are presented as functions of the powder densities, compositions, process feed rates and velocities, and area fractions in the solidified cladding bead.

Carbide Powder Efficiency

Carbide efficiency is the ratio of mass of carbide in the bead to mass of carbide in the powder feed:

$$\eta_{m_c} = \frac{m'_{c_b}}{m'_{c_p}} \quad (1)$$

where η_{mc} is the carbide catchment efficiency, m'_{cb} is the linear mass density of carbide in the clad bead, and m'_{cp} is the linear mass density of carbide in the powder feed.

The linear mass density of carbide in the bead is given by

Table 4 — Carbide, Metal Powder, and Overall Catchment Efficiency for the Experimental Cladding Beads

Bead Number	Carbide Efficiency η_{mc} (%)	Metal Powder Efficiency η_{mm} (%)	Overall Efficiency η_m (%)
Bead 1	53.23	73.39	60.77
Bead 2	18.15	32.11	23.37
Bead 3	36.14	67.07	47.71
Bead 4	41.83	74.91	54.13
Bead 5	34.38	77.65	50.56
Bead 6	36.87	52.48	42.67
Bead 7	41.73	60.81	48.87
Bead 8	37.75	46.70	41.10
Bead 9	52.01	74.92	60.58
Bead 10	45.16	59.65	50.58
Bead 11	48.33	57.97	51.94
Bead 12	31.46	40.73	34.93
Bead 13	45.56	55.71	49.36

$$m'_{c_b} = f_{v_{c_b}} A_{b_T} \rho_c \tag{2}$$

where f_{vcb} is the volume fraction of carbide in the bead, A_{bT} is the total cross-sectional area of the bead, and ρ_c is the density of the carbide. f_{vcb} and A_{bT} are measured from the image cross section, and ρ_c is calculated from crystallographic analysis of the unit cell shown in Appendix A.

Equation 2 is valid when the distribution of carbides is isotropic, and the volume fraction of carbides is the same as the area fraction of any cross section. The total cross-sectional area of the bead A_{bT} is subdivided into the reinforcement area A_{bR} above the surface level as a result of mass addition from the process, and the dilution area A_{bD} due to the mixing of the steel substrate and molten metal powders to create a metallurgical bond. These areas are shown in Fig. 1. A_{bT} appears in Equation 2 to account for carbides that can settle below the surface during solidification. In laser cladding processes, A_{bD} is small compared to A_{bR}, typically less than 5% of the total bead area and has been reported to be as low as 1–2% (Ref. 12).

The mass of carbide in the powder is given by

$$m'_{c_p} = \frac{f_{m_{c_p}} \dot{m}_p}{V_t} \tag{3}$$

where f_{mcp} is the weight fraction of carbide in the powder feed, which is measured directly while weighing each component during in-house blending of the carbide and metal powders $\dot{m}_p$ is the total mass transfer rate of the powder feed, which is determined after a two-minute particle collection test and weight measurement, and V_t is the substrate travel speed, which is not directly measured and taken as exact from the program input into a high-precision CNC positioner.

Substituting Equations 2 and 3 into Equation 1, the carbide efficiency can be calculated from measured quantities as

$$\eta_{m_c} = \frac{V_t A_{b_T} \rho_c}{\dot{m}_p} \frac{f_{v_{c_b}}}{f_{m_{c_p}}} \tag{4}$$

Metal Powder Efficiency

Metal powder efficiency is the ratio of mass of metal powder in the bead to mass of metal powder in the powder feed

$$\eta_{m_m} = \frac{m'_{m_b}}{m'_{m_p}} \tag{5}$$

where η_{mm} is the metal powder catchment efficiency, m'_{mb} is the linear mass density of metal powder in the clad bead, and m'_{mp} is the linear mass density of metal powder in the powder feed.

The mass of metal powder in the bead is given by

$$m'_{m_b} = \left(1 - f_{v_{c_b}}\right) A_{b_R} \rho_m \tag{6}$$

where ρ_m is the density of the metal powder reported from the powder manufacturer.

In Equation 6, A_{bR} appears instead of A_{bT} to account for only the addition of mass from the process. This distinction excludes the bead area contribution from dilution that was existing mass prior to cladding; however, with A_{bD} on the order of 1–2%, A_{bR} can be considered the same as A_{bT} for controlled cladding processes.

The mass of metal powder in the total powder/carbide mix is given by

$$m'_{m_p} = \frac{f_{m_{m_p}} \dot{m}_p}{V_t} \tag{7}$$

where f_{mmp} is the weight fraction of metal powders in the powder feed, which is measured directly while weighing each component during in-house blending of the carbide and metal powders.

Substituting Equations 6 and 7 into Equation 5, the metal powder efficiency can be calculated from measured quantities as

$$\eta_{m_m} = \frac{V_t A_{b_r} \rho_m}{\dot{m}_p} \frac{\left(1 - f_{v_{c_b}}\right)}{f_{m_{m_p}}} \tag{8}$$

Overall Powder Efficiency

Overall efficiency is the ratio of the carbide and metal powders in the bead to the total amount of powders exiting the cladding head

$$\eta_m = \frac{m'_{c_b} + m'_{m_b}}{\dot{m}_p / V_t} \tag{9}$$

where η_m is the overall powder efficiency.

Substituting Equations 4 and 6 into Equation 9, the overall powder efficiency can be calculated from measured quantities as

$$\eta_m = \frac{V_t}{\dot{m}_p} \left[\begin{matrix} A_{b_T} f_{v_{c_b}} \rho_c + A_{b_r} \\ \left(1 - f_{v_{c_b}}\right) \rho_m \end{matrix} \right] \tag{10}$$

Results

The calculation of efficiency requires the total area of the bead, the reinforcement area, and volume fraction of carbide in the deposited cladding, which all come from cross sections of the experimental beads.

Table 5 — Range of Variations Used for the Error Propagation Analysis

Variable	Range of Variation *a*	Comments
q	± 5.5%	Reported uncertainty from the manufacturer of the power probe
m_p	± 0.01%	Reported uncertainty from the calibration certificate of the 6000-g scale
t_p	± 0.22 s	Reported uncertainty in operator reaction time from Kosinski analysis of reaction time (REF. 14)
V_t	0	Assumed to be negligible from high precision CNC positioner
A_{bT}	± 1%	Variation in measurements of pixel area between the sum of A_{bR}, A_{bD}, and A_{bT} directly
l_{sc}	± 0.01 mm	Resolution of the microscope calibration scale
l_{sm}	± 5%	Variation in repeat measurements of scale bar in Photoshop™
ρ_c	± 82.5 kg/m^3	Selected as half the range of Fig. 8
$f\upsilon_{cb}$	± 5 %	Variation in measurements from the Python™ script
fm_{cp}	± 5%	Variation in measurements from the Python™ script
m_c	± 0.01%	Reported uncertainty from the calibration certificate of the 200-lb scale
m_m	± 0.01%	Reported uncertainty from the calibration certificate of the 200-lb scale
A_{bR}	± 1%	Selected to be consistent with A_{bT}. In most cases $A_{bR} \approx A_{bT}$
ρ_m	0	Assumed to be negligible from the reported manufacturer value

Figure 3 shows a typical cross section of a Ni-WC cladding.

Occasionally, small sintered particles outside of the main bead were observed, such as the one shown on the left side of the bead in Fig. 3. These sintered powders do not contribute to the buildup of the main bead and are not considered as part of this analysis of efficiency for single beads. Voids in the cladding were also occasionally observed and were typically accounted for as matrix material in the calculations. This is a reasonable approximation for beads with low porosity such as those in these experiments. Figure 3 shows a void on the left side of the bead likely caused by a carbide being pulled out during the sample preparation process based on its size. Figure 4 shows the output of the Python™ script highlighting the carbide area. The colors are randomly generated by the program.

Table 3 summarizes the area and carbide fraction measurements from all experimental clads. Using the data from Tables 2 and 3 and Equations 4, 8, and 10, the carbide, metal powder, and overall efficiency were determined for all experiments. These efficiencies are summarized in Table 4.

The trends in efficiency for carbide, metal powder, and overall were analyzed by separating the calculated efficiencies from the cladding experiments into the three test blocks for power, powder feed rate, and substrate travel speed. Figures 5, 6, and 7 show the effects of power, powder feed rate, and travel speed on catchment efficiency of the experimental cladding beads. The uncertainty for the calculated values of catchment efficiency was estimated from error propagation of Equations 4, 8, and 10 using standard techniques described in the NIST handbook on statistical methods (Ref. 13). For this error propagation analysis, Table 5 summarizes the range of variation of each variable involved (±a). For all variables, a uniform probability distribution in the range of variation was assumed as a conservative estimate (Ref. 13). The standard deviation is therefore $1/\sqrt{3}a$. The t-statistic for a two-tailed test with infinite degrees of freedom for the 95% confidence level is 1.960.

Figure 5 shows increasing laser power increases both the carbide and metal efficiency. The linear trend lines in the graph aim to capture the overall behavior of catchment; these lines are not models or an attempt to represent a particular physical phenomenon. The trend lines indicate that the overall catchment efficiency increases approximately 17%/kW for the conditions tested.

Figure 6 shows that metal powder efficiency decreases with powder feed rate (~0.45%/g/min), while carbide efficiency increases (~0.22%/g/min). The smaller effect on carbide efficiency was on the order of the confidence interval and further work is needed to confirm this trend. For the values measured, the overall catchment efficiency was nearly insensitive to powder feed rate. It is important to highlight that while overall efficiency was approximately constant, carbide fraction varied in a measurable way (carbide fraction increased with powder feed rate). This carbide fraction is of high importance for the quality and performance of the cladding.

Figure 7 shows that increasing travel speed decreases the carbide, metal powder, and overall efficiencies. The overall efficiency shows a decreasing trend of 1%/mm/s with a total ~25% decrease in efficiency for the conditions tested.

Discussion

Increasing laser power demonstrated a rise in carbide, metal powder, and total efficiency, which is most likely due to increased molten pool size with higher power density. There is also likely an increase in particle preheat, which contributes to increased efficiency as observed by Kumar and Roy (Ref. 15). In practice, there is a limit to the effectiveness of the carbide efficiency increase at high power levels, as the heat-sensitive carbides dissolve and reprecipitate brittle phases on their surfaces, which degrades wear performance (Ref. 1).

For the powder feed rate test block, the decreased trend in metal powder efficiency and increased trend in carbide efficiency with increased feed rate can be exploited to manipulate the carbide fraction in the deposited cladding. Despite the negligible change in overall efficiency on a percentage basis, this behavior would be limited in practice by the likelihood of disbonding the cladding from the substrate.

The observed decrease in carbide, metal powder, and overall efficiency with increased travel speed was consistent with the linearly decreasing approximation by Colaço et al. (Ref. 16). This trend is likely due to the de-

creased interaction time between the laser beam and the substrate, which decreases the molten pool size. This explanation is supported by the decrease in width and height of beads with increasing travel speed shown by several sources (Refs. 8, 16, and 17).

For all experiments, the metal powder efficiency was higher than the carbide, which is consistent with favorable wetting of the primarily nickel powder to the molten nickel pool. This explanation is supported by the findings of Guest et al., who observed carbide ricocheting off the surface of a molten nickel weld pool during gas metal arc welding of Ni-WC (Ref. 18).

Some important assumptions were made in this work that are addressed here. It was assumed that the area fraction of a single cross section was representative of the bead volume. This assumption is typically made because of the long preparation time required for each individual sample. In measuring the carbide efficiency, pores or voids were occasionally observed in the cross section, which were included in the calculations as matrix area. These voids were not regularly observed and can be reasonably assumed to have a negligible effect on the reported trends in this work. The Python™ program occasionally missed tracking carbides, and the carbide fractions measured are a lower bound. Because very few carbides are omitted, the measurements are taken as representative of the actual carbide fraction.

Finally, the dilution of carbides in the matrix was neglected; this is reasonable because reprecipitated carbides were not observed in any sample.

The accuracy of the Python measurements could possibly be improved by discriminating porosity due to shrinkage from that of pulled-out carbides during sample preparation. Shrinkage porosity has a rough and irregular shape, while gas porosity and pulled-out carbides have round shapes. Gas porosity and pulled-out carbide can be further discriminated due to the presence of a smooth diffuse reflection in voids related to gas porosity.

While the developed equations for component efficiency were demonstrated using the Ni-WC system, this method could be extended to any two-component powder feed system with the same distinct components in the powder feed and deposited bead. The same equations would also be valid using off-axis powder feeding, as typically done for ID applications, and so they are not exclusive to coaxial cladding.

Conclusions

This work has evaluated for the first time the individual efficiencies for a dual-component powder feed made of tungsten carbide and metal powders. Preliminary experimental data for single beads of the Ni-WC powder mixture deposited using a 6-kW CO_2 laser indicated the following:

1) Increasing laser power increased carbide, metal powder, and overall efficiency.

2) Power feed rate had a minimal effect on overall efficiency, but demonstrated a simultaneous decrease in metal powder efficiency with an increase in carbide efficiency. This behavior is relevant to controlling the carbide fraction in the deposited cladding.

3) Increasing travel speed showed strong decreases in carbide, metal powder, and overall efficiency.

4) In all cases the metal powder efficiency was observed to be higher than the carbide.

Acknowledgments

The authors wish to acknowledge the helpful comments and suggestions from Doug Hamre, head of research and development at Apollo Clad Laser Cladding, a division of Apollo Machine and Welding, Ltd. Apollo was instrumental in sharing its knowledge, equipment, and powder blends. The authors also acknowledge NSERC for providing project funding for this research. Student scholarships from the American Welding Society and Canadian Welding Association were gratefully received.

Appendix A

Tungsten Carbide Density

The density of carbide ρ_c was calculated using the mass and volume of the unit cell ($\rho_c = m_c/V_c$). The crystallography of WC_{1-x} is the cubic "rock salt" B1-type (Ref. 19). For this type of carbide (MC_{1-x} where M stands for metal), the variation in stoichiometry arises from structural vacancies in the nonmetallic sites (Ref. 20), namely C for WC_{1-x}.

The mass of the unit cell is then

$$m_c = \frac{N_W M_W + N_C M_C (1-X)}{N_a} \quad (11)$$

where m_c is the mass of the WC_{1-x} unit cell, $N_{W=4}$ is the number of W atoms in the unit cell, M_W is the molar mass of W, $N_C = 4$ is the number of C atoms in the unit cell, M_C is the molar mass of C, (1–X) is the stoichiometry of C in the W_{C1-x} phase, and N_A is Avegadro's number.

The volume of the unit cell is given by $Vc = a_{B1}{}^3$ where V_c is the volume of the WC_{1-x} unit cell, and a_{B1} is the lattice parameter of the same unit cell. Kurlov and Gusev have investigated the unit cell lattice parameters reported in literature and developed a best-fit quadratic to represent the change in lattice parameter as a function of carbon content in the WC_{1-x} structure (Ref. 21).

$$a_{B1} = 0.4015 + 0.0481(1-X) - 0.0236\,(1-X)^2 \quad (12)$$

The final form of the theoretical density of WC_{1-x} is then

$$\rho_c = \frac{N_W M_W + N_c M_c (1-X)}{N_A \left[\begin{array}{l} 0.4015 + 0.0481(1-X) \\ -0.0236(1-X)^2 \end{array} \right]^3} \quad (13)$$

WC_{1-x} has a homogeneity region between (1–X) = 0.59 and (1–X) = 1.00 (Ref. 22). Using Equation 13, the density of WC_{1-X} was determined for the entire homogeneity region shown in Fig. 8. For the carbides involved in this work, (1–X) = 0.604 corresponding to a density of 16,896 kg/m^3.

References

1. Mendez, P. F., Barnes, N., Bell, K., Borle, S. D., Gajapathi, S. S., Guest, S. D., Izadi, H., Kamyabi Gol, A., and Wood, G. 2013. Welding processes for wear resistant overlays. *Journal of Manufacturing Processes* 16: 4–25.

2. Guest, S. D. 2014. Depositing Ni-WC wear resistant overlays with hot-wire assist technology. PhD thesis, University of Alberta, Canada.

3. Lin, J. 1999. A simple model of powder catchment in coaxial laser cladding. *Optics & Laser Technology* 31: 233–238.

4. Picasso, M., Marsden, C. F., Wagnière, J. D., Frenk, A., and Rappaz, M. 1994. A simple but realistic model for laser cladding. *Metallurgical and Materials Transactions B* 25B: 281–291.

5. Lin, J., and Steen, W. M. 1997. Powder flow and catchment during coaxial laser cladding. *Laser in Materials Processing*, vol. 2097, pp. 517–524. The International Society for Optical Engineering.

6. Frenk, A., Vandyoussefi, M., Wagnière, J. D., Zryd, A., and Kurz, W. 1997. Analysis of the laser cladding process for stellite on steel. *Metallurgical and Materials Transactions B* 28B: 50–508.

7. Partes, K. 2009. Analytical model of the catchment efficiency in high speed laser cladding. *Surface & Coatings Technology* 204: 366–371.

8. de Oliveira, U., Ocelík, V., and De Hosson, J. Th. M. 2005. Analysis of coaxial laser cladding processing conditions. *Surface and Coatings Technology* 197: 127–136.

9. Gremaud, M., Wagnière, J. D., Zyrd, A., and Kurz, W. 1996. *Laser Metal Forming: Process Fundamentals. Surface Engineering* 12(3): 251–259.

10. Zhou, S., Huang, Y., and Zeng, X. 2008. A study of Ni-based WC composite coatings by laser induction hybrid rapid cladding with elliptical spot. *Applied Surface Sciences* 254: 3110–3119.

11. Angelastro, A., Campanelli, S. L., Casalino, G., and Ludovico, A. D. 2013. Optimization of Ni-based WC/Co/Cr composite coatings produced by multilayer laser cladding. *Advances in Materials Science and Engineering*, pp. 1–7.

12. St-Georges, L. 2007. Development and characterization of composite Ni-Cr + WC laser cladding. *Wear* 263: 562–566.

13. NIST/SEMATECH e-Handbook of Statistical Methods. 2013. *http://www.itl.nist.gov/div898/handbook/*.

14. Kosinksi, R. J. 2013. A literature review on reaction time.

15. Kumar, S., and Roy, S. 2006. Development of theoretical process maps to study the role of powder preheating in laser cladding. *Computational Materials Science* 37: 425–433.

16. Colaço, R., Costa, L., Guerra, R., and Vilar, R. 1996. A simple correlation between the geometry of laser cladding tracks on the process parameters. *Laser Processing: Surface Treatment and Film Deposition*, pp. 421–429. Kluwer Academic Publishers, Netherlands.

17. Cheikh, H. E., Courant, B., Hascoët, J.-Y., and Guillén, R. 2012. Prediction and analytical description of the single laser track geometry in direct laser fabrication from process parameters and energy balance reasoning. *Journal of Materials Processing Technology* 212: 1832–1839.

18. Guest, S. D., Chapuis, J., Wood, G., and Mendez, P. F. 2014. Non-wetting behaviour of tungsten carbide powders in nickel weld pool: new loss mechanism in GMAW overlays. *Science and Technology of Welding and Joining* 19(2): 133–141.

19. Kurlov, A. S., and Gusev, A. I. 2013. Phases and equilibria in the W-C and W-Co-C systems. *Tungsten Carbides: Structure, Properties and Application in Hardmetals*, pp. 5–56. Springer International Publishing, Switzerland.

20. Rempel, A. A. 1996. Atomic and vacancy ordering in nonstoichiometric carbides. *Physics – Uspekhi* 39(1): 31–56.

21. Kurlov, A. S., and Gusev, A. I. 2010. Phase equilibria in the W-C system and tungsten carbides. *Russian Chemical Reviews* 75(7): 617–636.

22. Sara, R. V. 1965. Phase equilibria in the system tungsten-carbon. *Journal of The American Cermaic Society* 5: 251–257.

Statement of Ownership, Management and Circulation for U.S. Postal Service (Required by U.S.C. 3685)

1. TITLE OF PUBLICATION: Welding Journal
2. PUBLICATION NO.: ISSN 0043-2296
3. DATE OF FILING: September 28, 2015
4. FREQUENCY OF ISSUE: Monthly
5. NO. OF ISSUES PUBLISHED ANNUALLY: 12
6. ANNUAL SUBSCRIPTION: $120.00
7. MAILING ADDRESS OF KNOWN OFFICE OF PUBLICATION: 8669 NW 36 St., #130, Miami, Florida 33166
8. MAILING ADDRESS OF THE HEADQUARTERS OR GENERAL BUSINESS OFFICES OF THE PUBLISHERS: 8669 NW 36 St., #130, Miami, Florida 33166
9. NAMES AND COMPLETE ADDRESS OF PUBLISHER, EDITOR AND MANAGING EDITOR:
   PUBLISHER: Andrew Cullison, AWS, 8669 NW 36 St., #130, Miami, Florida 33166
   EDITOR: Mary Ruth Johnsen, AWS, 8669 NW 36 St., #130, Miami, Florida 33166
10. OWNER: NAME: American Welding Society, Inc. ADDRESS: AWS, 8669 NW 36 St., #130, Miami, Florida 33166
11. KNOWN BONDHOLDERS, MORTGAGEES, AND OTHER SECURITY HOLDERS OWNING OR HOLDING 1 PERCENT OR MORE OF TOTAL AMOUNT OF BONDS, MORTGAGES OR OTHER SECURITIES: None
12. The purpose, function, and nonprofit status of this organization and the exempt status for Federal income tax purposes: Has not changed during preceding 12 months
13. Publication Title: Welding Journal
14. Issue date for Circulation Data Below: October 2015
15. EXTENT AND NATURE OF CIRCULATION:

	Average No. Copies Each Issue During Preceding 12 Months	Actual No.Copies of Single Issue Published Nearest to Filing Date
A. Total No. Copies Printed (Net Press Run)	53,716	56,500
B. Paid and/or Requested Circulation		
1. Paid / Requested Outside-County Mail Subscriptions Stated on Form 3541	51,841	52,023
2. Paid In-County Subscriptions Stated on Form 3541	None	None
3. Sales Through Dealers and Carriers, Street Vendor, Counter Sales, and other Non-USPS Paid Distribution	None	None
4. Other Classes Mailed Through the USPS	None	None
C. Total Paid / Requested Circulation	51,841	52,023
D. Free Distribution by Mail (Samples, complimentary and other free)		
1. Outside-County as State on Form 3541	178	179
2. In-County as Stated on Form 3541	None	None
3. Other Classes Mailed Through the USPS	None	None
4. Free Distribution Outside the Mail (Carriers or other means)	None	None
E. Total Free Distribution	178	179
F. Total Distribution	52,019	52,202
G. Copies not Distributed	1,698	4,298
H. Total	53,717	56,500
I. Percent Paid and / or Requested Circulation	99.7%	99.7%

16. Statement of Ownership will be printed in the November 2015 issue of this publication.
I certify that the statements made by above are correct and complete:
Mary Ruth Johnsen, Editor